Acta Cryst. (1999). B**55**, 297–305

Arrangement of C atoms in the SiC–C solid solution

O. O. Mykhaylyk* and M. P. Gadzira

Institute for Problems of Materials Science, Ukrainian National Academy of Sciences, Krzhyzhanivskogo 3, 252180 Kyiv, Ukraine. E-mail: oom65@usa.net

(*Received 27 April 1998; accepted 26 October 1998*)

Abstract

The microstructure of a silicon carbide–carbon solid-solution powder (SiC–C), obtained from a fine powder of silicon and thermal expansive graphite, is investigated by X-ray powder diffraction methods. The microstructure is characterized by Williamson–Hall analysis and the strain-field model suggested by van Berkum *et al.* [*Acta Cryst.* (1996), A**52**, 730–747]. SiC–C adopts a layered structure like the solid solutions formed by compounds possessing a diamond-like structure, *e.g.* SiC–AlN. Superstoichiometric C atoms are located as planar defects. The SiC–C solid solution is destroyed on heating in a vacuum in the temperature range of graphitization of diamond but is maintained after sintering at high pressure (4–8 GPa) and high temperature (1673 and 2073 K). However, at the higher temperature (2073 K), it is observed that planar defects formed by C atoms decompose to non-correlated point defects accompanied simultaneously by a decrease in the lattice parameter from 4.3540 (2) to 4.35234 (5) Å.

1. Introduction

Under equilibrium conditions there is only one compound in the Si–C system: SiC (Olesinski & Abbaschian, 1984). SiC exists in a number of different polytypic forms. Lely (1955) stated that the compound deviates slightly (10^{-5} at.%) from the stoichiometric composition SiC. However, further investigations (Shaffer, 1969; Sorokin *et al.*, 1983) showed that, depending on the polytype of SiC, the composition can vary in the direction of excess silicon within the limits $1 < \mathrm{Si{:}C} < 1.049$. On the basis of data concerning the decrease in the lattice parameter of SiC [a = 4.347 (1) Å†] compared with the tabulated value [a = 4.3589 (1) Å‡], von Bonnke & Fitzer (1966) argued that a silicon carbide with superstoichiometric carbon is formed owing to the substitution of some Si atoms by C. Recently, a similar conclusion was reached based on microhardness data (sintered samples have a microhardness of 40 GPa), Raman spectra and a determination of the lattice parameter [a = 4.353 (1) Å; Gadzyra *et al.*, 1996]. Indeed, the very high microhardness compared with standard β-SiC (∼29 GPa) may point to the presence of sp^3 C—C bonds in the SiC structure.

This conclusion agrees with the theoretical work of Wang *et al.* (1988), in which it is shown that of all the native defects of the SiC structure leading to a decreased lattice parameter (carbon vacancies, V_C, silicon vacancies, V_{Si}, and carbon anti-sites, C_{Si}), C_{Si} (C atoms occupying Si sublattice sites) have the minimum energy. Although silicon carbide and carbon (diamond) have the same crystal structure and a similar type of bonding for forming a solid solution, these results are not expected since the atomic sizes of Si and C are significantly different (the covalent radii of Si and C are 1.17 and 0.72 Å, respectively).

We believe that the silicon-carbide structure imperfections observed in the studies described above are connected either with the unusual nature of the chemical-vapour deposition process used by von Bonnke & Fitzer (1966), in which a periodic alternation of the composition of a deposited gas mixture creates a coherently connected layer crystal structure, or the unusual structural state of carbon used by Gadzyra *et al.* (1996), thermal expansive graphite (TEG) (compared with, for example, graphite, carbon black or pyrolyzed hydrocarbon, which are normally used for silicon carbide synthesis), in which separate graphite layers have a thickness of not more than a few atomic planes (Yurkovskii *et al.*, 1986). However, studies of the mechanism of formation of the SiC–C solid solution and the arrangement of the superstoichiometric carbon in silicon carbide have not been carried out. In this work, therefore, we pay principal attention to the microstructural characteristics of an as-synthesized SiC–C solid solution and the behaviour of the solid solution under different high-temperature and high-pressure treatments.

2. Experimental

The SiC–C solid-solution powder was synthesized in a Tamman furnace by heating a mixture of a fine powder of semiconductor-pure elemental silicon and TEG

† This value was estimated from a plot presented by von Bonnke & Fitzer (1966).

‡ Powder Diffraction File No. 29-1129; the wavelength for Cu $K\alpha$ radiation was taken to be 1.54178 Å [$\lambda(K\alpha_1)$ = 1.54051 Å].

Table 1. *Strains (e_{WH}) and lattice parameters (a) of the β-SiC–C solid-solution powder after different treatments*

Treatment conditions	$e_{WH} \times 10^3$	a (Å)
As synthesized	0.99 (6)	4.3540 (2)
Annealed		
At 1673 K	0.77 (6)	4.3542 (2)
At 1873 K	0.72 (5)	4.3564 (2)
At 1973 K	0.49 (4)	4.35899 (8)
Sintered at high pressure and 1673 K		
4 GPa†	2.59 for <001> and 1.48 for <111>	4.3544 (3)
8 GPa†	4.31 for <001> and 3.5 (2) for others	4.3545 (4)
Sintered at high pressure and 2073 K		
8 GPa†	0.67 for <001> and 0.22 for <111>	4.35362 (6)
6 GPa	0.39 (4)	4.35313 (6)
4 GPa	0.09 (2)	4.35234 (5)

† e_{WH} was calculated for different crystallographic directions of the β-SiC structure owing to strain anisotropy.

produced from sulfuric graphite (weight ratio Si:C = 2.33:1) to 1573 K under argon. The unreacted carbon which remained in the sample after the synthesis was removed by heating the sample in air at 923 K followed by HF etching to remove silicon oxide. Details of the preparation of the SiC–C powder have been given elsewhere (Gadzyra *et al.*, 1996).

The SiC–C solid-solution powder was treated further under different conditions (see Table 1):

(i) Annealing in a vacuum furnace (10 Pa) in the temperature range 1673–2073 K.

(ii) Sintering for 60 s at 1673 and 2073 K and at high pressure (4–8 GPa) using 'toroid'-type high-pressure equipment composed of a pyrophyllite container with graphite heater and NaCl pressure medium.

Powder diffraction data were collected using a DRON-UM1 powder diffractometer [with a 192 mm goniometer radius, Cu $K\alpha$ radiation, $\lambda(K\alpha_1)$ = 1.5405981 Å, and a graphite diffracted-beam monochromator]. The divergence of the incident beam was 0.6° and the receiving-slit width was 0.015 or 0.15°. Throughout the experiment the ambient temperature was maintained at 293 (1) K.

The position (2θ), full width at half-maximum (FWHM) and the shape of individual Bragg reflections were obtained using the *CSD* program package (Akselrud *et al.*, 1989). Line profiles were modelled by a pseudo-Voigt function; asymmetric parameters were not necessary as almost all the lines were effectively symmetrical. The pseudo-Voigt function is defined as $\mathrm{pV}(x) = \eta L(x) + (1 - \eta)G(x)$, where $L(x)$ and $G(x)$ are the Lorentzian and Gaussian functions, respectively, and the parameter η ($0 \leq \eta \leq 1$) is the mixing ratio of $L(x)$ and $G(x)$. The *CSD* package was also used for a least-squares refinement of the unit-cell parameters. The shifts of diffraction lines caused by the displacement of the specimen surface from the goniometer axis were taken into account in the calculations.

The adjustment of the diffractometer was checked using silicon (semiconductor pure, annealed at 1463 K, particle size < 10 μm) and β-SiC [a fine powder synthesized by the reaction of SiO_2 and C (Khaenko *et al.*, 1995), which was annealed up to 2063 K to achieve a stacking-fault-free structure]. The lattice parameters determined for these materials were 5.43080 (7) and 4.35903 (5) Å, respectively. Since the linear absorption coefficients of SiC and Si are high ($\mu_{Si} \simeq \mu_{SiC} \simeq 14\ \mathrm{mm}^{-1}$), the effect of transparency on the peak positions is negligible for single crystals. However, this is not the case for powders. In our case, the density of the powder specimens prepared for diffractometry was nearly 40% of the theoretical density. Therefore, the effective value of μ was only $\sim 5.6\ \mathrm{mm}^{-1}$ and the necessary corrections for the peak positions were made.

The microstructural properties of the SiC–C solid-solution samples were characterized by the dependence of the integral breadths β_f, which were corrected for instrumental broadening. The annealed β-SiC powder mentioned above was used as an instrumental standard (Fig. 1). Warren–Averbach analysis (Warren, 1969) or another Fourier method can yield more detailed information on the microstructure than methods based on breadth parameters, since a set of Fourier coefficients represents a line profile in all its details (van Berkum *et al.*, 1996). These methods of line-broadening analysis using line profiles of pairs of reflections of different orders, such as 111 and 222 or 002 and 004, are, in principle, suitable in the case of the cubic β-SiC structure. However, they can only be used for well resolved peaks. In our case, the overlapping tails of the 111 and 002 line profiles (see Fig. 2) and the satellite peak at d = 2.66 Å made them unsuitable. Therefore, only Williamson–Hall analysis (Williamson & Hall, 1953) based on the width parameters was used. In this analysis it is assumed that $\beta_f(d^*) = \beta^S + \beta^D(d^*)$, where β^S ($= 1/D_{WH}$) is d^*-independent size broadening and β^D

$[= (2\pi)^{1/2} e_{WH} d^*]$ is d^*-dependent strain broadening ($d^* = 2\sin\theta/\lambda$). D_{WH} and e_{WH} ($= \Delta d/d$) are size and strain parameters, respectively. Therefore, a straight line in a plot of $\beta_f(d^*)$ *versus* d^* will give $1/D_{WH}$ and $(2\pi)^{1/2} e_{WH}$ as the intercept and slope, respectively. If β_f has both 'size' and 'strain' contributions Williamson–Hall analysis should not be used quantitatively, other than as a first approximation, since β^S and $\beta^D(d^*)$ are linearly additive only when the corresponding line profiles are Lorentzian. In other cases this assumption gives systematic errors. Nevertheless, this type of analysis and plot give a valuable insight into the nature of any structure imperfections present.

Before the investigation of microstrain, the presence of residual stress (macrostrains) in the sintered materials was estimated. The ψ-goniometer method was used, where ψ is the angle between the normal to the specimen surface and the normal to the reflecting plane. The difference between the spacing of planes reflecting in the high-angle area (224 and 333, 115) measured at $\psi = 0$ and $\psi = \pm 30^\circ$ was close to zero (not more than 10^{-4} Å). Thus, macrostrains did not appear in the sintered specimens and therefore did not add to the broadening of the diffraction peaks.

3. Results and discussion

3.1. *As-synthesized SiC–C solid-solution powder*

The diffraction pattern of the as-synthesized SiC–C solid-solution powder (after cleaning) showed very weak peaks which could belong to α-Si_3N_4, Si_2N_2O and graphite. All intense lines corresponded to the face-centred-cubic silicon carbide structure. Only one reflection in the low-angle area of the 111 β-SiC peak (Fig. 2) was not indexed. According to the literature (Tateyama *et al.*, 1988; Pujar & Cawley, 1995) this additional peak at $d = 2.66$ Å is connected with stacking faults in the β-SiC structure. This suggestion is also confirmed by the high background intensity around the 111 β-SiC peak (Fig. 2) and relative intensities of peaks which differ from those predicted for the perfect β-SiC structure (for example, $I_{111}/I_{002} = 5.6$ for perfect β-SiC and $I_{111}/I_{002} = 8.4$ for our powder). However, the presence of α-SiC polytypes (2*H*, 4*H*) with stacking faults which have an allowed reflection 010 (indexed on hexagonal axes for the α-SiC structure) with $d = 2.66$ Å is not excluded.

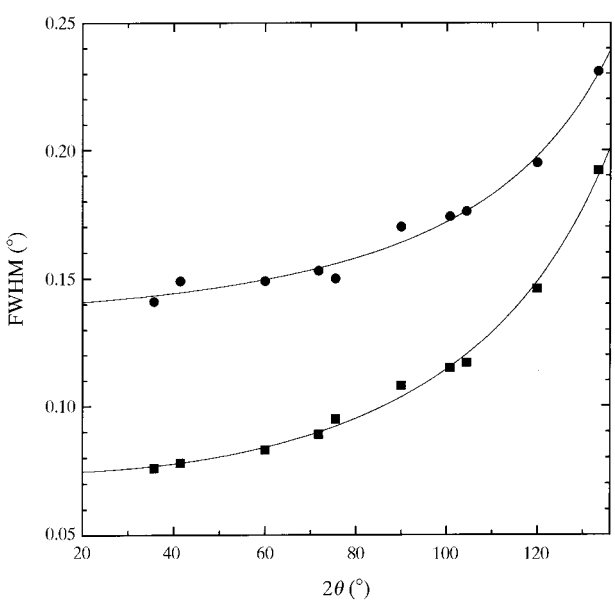

Fig. 1. FWHM *versus* 2θ for diffraction lines of standard β-SiC. ■ slit width 0.015° 2θ; ● slit width 0.15° 2θ; solid line: the instrumental resolution curve of the diffractometer. The interpolation was carried out by least-squares refinement using the Cagliotti approximation ($FWHM^2 = U\tan^2\theta + V\tan\theta + W$).

In a general classification (Warren, 1969), the stacking faults are divided into twin faults and deformation faults (intrinsic and extrinsic). The latter cause *hkl*-dependent peak shifts, which lead to significant errors when the unit-cell parameter is calculated. However, in our case the $\sin\theta_{002}/\sin\theta_{111}$ ratio† was equal to 1.155 (1) and did not differ from the theoretical value. Thus, only twin faults which do not shift the peak positions are present in the structure of the as-synthesized silicon carbide powder. This allowed us to refine the SiC–C solid-solution lattice parameter more exactly. Such conclusions were also made for the annealed and sintered samples.

The lattice parameter of the as-synthesized silicon carbide was found to be smaller than for standard β-SiC (see Table 1). This decrease in the lattice parameter, inappropriate for stoichiometric β-SiC, showed the presence of first-class defects [according to the classification suggested by Krivoglaz (1996)] in the structure of the as-synthesized silicon carbide, namely point defects and, in particular, carbon anti-sites. The atomic displacements produced by these defects decrease asymptotically as the square of the increasing distance in the crystal and do not produce broadening of lines in the X-ray diffraction pattern.

A Williamson–Hall plot showed that the integral width of seven out of ten reflections of the as-synthesized SiC–C powder plotted *versus* d^* lie near a straight line (Fig. 3). The 002, 004 and 133 reflections deviate from this line. This *hkl*-dependent behaviour is a classic case of broadening owing to stacking faults in close-packed structures belonging to the cubic system. From the theory of stacking-fault broadening (Warren, 1969) these reflections only have components which have been broadened by faults, while the others are a superposition

† The ratio $\sin\theta_{002}/\sin\theta_{111} = 1.1547$ is constant for a cubic structure and does not depend on the lattice parameter, but it increases owing to deformation stacking faults leading to the displacement of the 111 and 002 peaks (Warren, 1969).

of both the 'sharp' unaffected and broadening components. The integral widths of these three reflections were not included in the straight-line approximation (Williamson–Hall analysis). The line has a small positive intercept with the ordinate (Fig. 3), *i.e.* the broadening owing to crystallite size [according to scanning electron microscopy the particle size is approximately 5000 Å; Gadzyra *et al.* (1996)] and the number of stacking faults is small. At the same time the d^*-dependent β_f behaviour is interpreted as being the result of strains (see Table 1) which could be produced by infinite-length second-class defects (dislocations, planar defects) according to the classification of Krivoglaz (1996). It should be noted that the pseudo-Voigt parameter η was 2θ-dependent and with increasing diffraction angle η changed from 0.9 to 0.3. The change of the profile from Lorentzian to Gaussian indirectly shows that the strain distribution is Gaussian, since the fraction of the strain-broadening component increases with 2θ.

The results presented here therefore confirm that both first- and second-class defects are present in the as-synthesized silicon carbide. However, the strong correlation of defects, resulting in their concentration along some preferred planes or lines in real crystals, can also change the X-ray scattering pattern. For instance, point defects located in preferred planes are, in a sense, equivalent to plane defects and produce broadening of the X-ray lines, like second-class defects (Krivoglaz, 1996). Therefore, the observed experimental data could in our case be described only by the presence of first-class (point) defects correlated with one another. This is the most reasonable approach for the interpretation of experimental data if the crystal-structure state of carbon used in the synthesis is to be taken into account.

TEG can be described as separate thin carbon layers consisting of a few graphite planes. On thermal treatment, the expansion of intercalated sulfuric graphite takes place by foliating of the crystal perpendicular to the *c* axis leading to the formation of a wrinkled structure (Yurkovskii *et al.*, 1986, or see Fig. 4*a*). A structural model of the separate fragments could be like that shown in Fig. 4*b*.

It is known that silicon carbide is formed on carbon components (*e.g.* Wei *et al.*, 1984) and it may be anticipated that in our case the formation of Si—C bonds on both sides of the thin carbon layer is equally plausible. Therefore, we believe that (i) such layered carbon

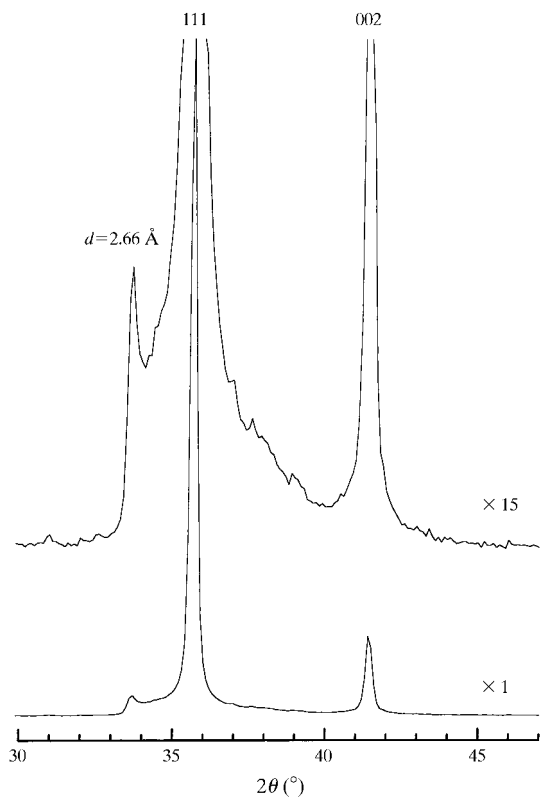

Fig. 2. The X-ray diffraction pattern of as-synthesized SiC–C solid-solution powder (× 1) and magnified (× 15). The reflections of cubic silicon carbide are indexed.

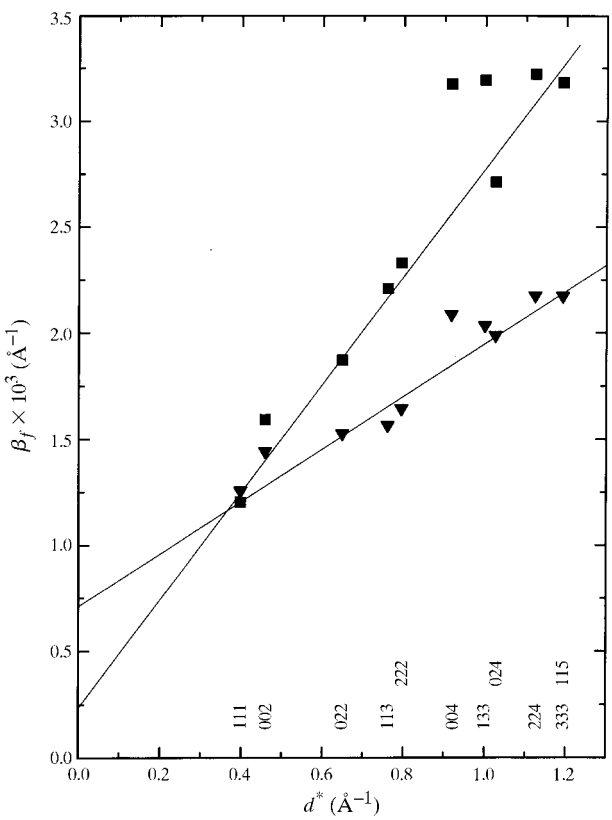

Fig. 3. The integral breadth β_f as function of d^* for line profiles (*hkl* given below) of as-synthesized SiC–C solid-solution powder (■) and the SiC–C powder annealed at 1973 K (▼). Straight-line fits to the seven data points (the 002, 004 and 133 reflections are excluded) have been used in the Williamson–Hall analysis.

structures (see Fig. 4*b*) persist in the reaction process and (ii) the graphite layers transform to a local diamond structure owing to formation of sp^3 bonds between carbon and silicon (see Fig. 5*a*). A layer structure similar to that described above has been observed in the SiC–AlN solid solution (Rafaniello *et al.*, 1981). Owing to the different C—C and Si—C distances, dislocations along the boundary between the carbon (C—C) layer and the silicon carbide (Si—C) layer should also be present. The latter is a source of strains in the as-synthesized SiC–C solid solution.

The considerably shorter interatomic C—C distance compared with Si—C therefore leads to the decrease of the lattice parameter; on the other hand, the carbon interlayers create strain fields causing the broadening of the diffraction lines. The suggested structural model of the SiC—C solid solution allows us to describe all the microstructural changes in the as-synthesized powder after different treatments.

3.2. *Annealed SiC–C solid-solution powder*

The microstructural parameters (strains, crystallite size and stacking faults) and lattice parameter of the SiC–C powder do not change after annealing for several hours at temperatures less than the synthesis

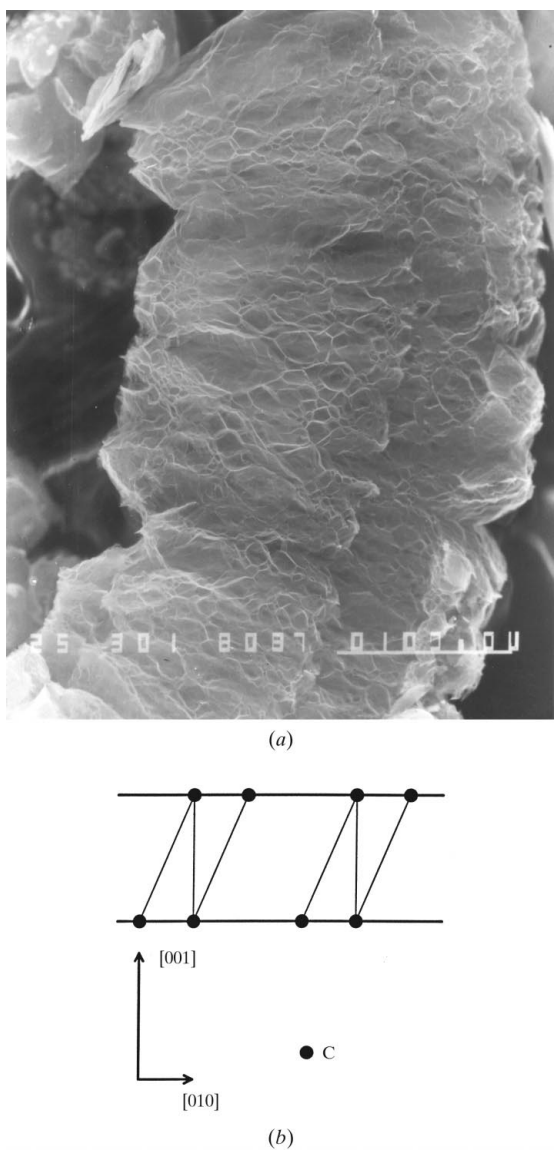

Fig. 4. (*a*) A scanning electron microscopy image of TEG. The scale bar corresponds to 100 μm. (*b*) A structural model of the separated graphite layer, cross section along (110).

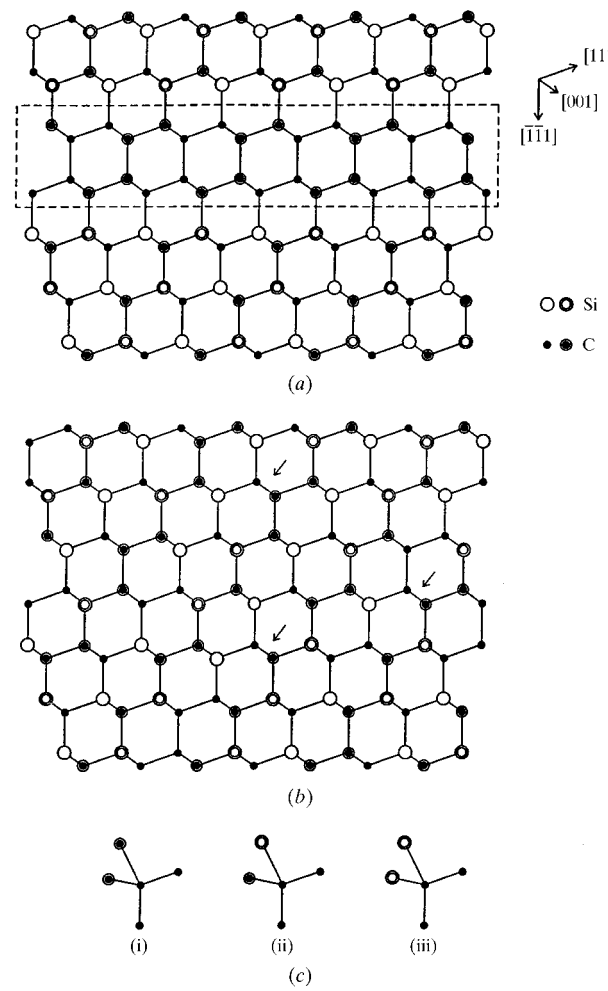

Fig. 5. A scheme of the SiC–C solid-solution crystal structure [projection onto $(1\bar{1}0)$]: (*a*) as-synthesized (dashed lines show the carbon interlayer), (*b*) after high-pressure sintering at 2073 K (arrows show the positions of the superstoichiometric C atoms after destruction of the interlayer) and (*c*) the probable local environments of the superstoichiometric C atoms in the SiC–C solid solution shown in part (*b*). Double-circled atoms lie out of the plane of the figure.

temperature (< 1473 K). However, at higher temperatures (starting at 1673 K) the lattice parameter increases (see Table 1) and achieves the standard value, characterizing β-SiC, at 1973 K and above. Such lattice-parameter behaviour indicates a reduction of the first-class (point) defect concentration in the silicon carbide structure.

Williamson–Hall microstructure analysis showed that the β_f dependence *versus* d^* for all annealed powders is approximated well by a straight line (Fig. 3) although, like the as-synthesized powder, deviations for three reflections (002, 004 and 133) were also observed (see §3.1). As the annealing temperature increases the strain parameter for the SiC–C structure decreases (see Table 1). Therefore, the annealing results in a reduction of the second-class (or similar) defects. In addition, the Williamson–Hall plot shows that the crystallite size decreases after annealing, while with increasing temperature this effect becomes greater and for the sample annealed at 1973 K (Fig. 3) D_{WH} = 1406 (156) Å. This is strange, since the resublimation process, leading to grain growth, will be more important with increasing temperature. D_{WH} is an apparent size and, in order to relate this to actual mean dimensions, some assumption about the morphology of the crystallites is required. If the morphology of the crystallites is spherical, then D_{WH} is related to the real diameter D by $D_{WH} = 3D/4$ (Wilson, 1962) and, therefore, D = 1875 (208) Å. This result is low in comparison with the real value, since the systematic errors connected with the stacking faults in the crystal structure were not taken into account in the calculations. However, the concentration of the stacking faults becomes considerably lower after annealing (the intensity of the satellite peak at d = 2.66 Å decreases and the ratio I_{111}/I_{002} decreases to 6.7).

Thus, three effects are observed simultaneously after the annealing of the as-synthesized SiC–C: (i) an increase of the lattice parameter, (ii) a decrease of the strains and (iii) a decrease of the crystallite size. In our opinion only one reasonable mechanism of structural behaviour could connect all these effects. On heating, the C—C diamond-like bonds in the carbon interlayers of the SiC–C structure break down. This will result in the destruction of the SiC–C particles along the planar carbon interlayers leading to the decrease of the crystallite size observed in the experiment. Such newly-formed particles do not have C—C sp^3 bonds already in the body; that is, the lattice parameter must increase compared to the normal value and the planar carbon defects in the structure creating the strain fields, namely the strain parameter e_{WH}, must decrease. This suggestion is confirmed by the fact that from 1670 K in a vacuum the processes of the natural diamond graphitization (the transformation of sp^3 C—C bonds to sp^2 bonds) are observed (Evans & James, 1964).

3.3. *SiC–C solid-solution powder sintered at high pressure and high temperature*

Unlike annealing in a vacuum, sintering at the same temperatures (1673 and 2073 K) but at high pressure, where diamond is more stable (Kennedy & Kennedy, 1976), does not lead to the breakdown of the SiC–C solid solution (the lattice parameter does not increase, see Table 1). However, the microstructural characteristics of the SiC–C are different and depend on the sintering conditions.

After sintering at 1673 K the lattice parameter does not change within the errors of the measurement (see Table 1). The Williamson–Hall plot (Fig. 6) shows that the β_f values for the reflections increase significantly with pressure. The spread of β_f for the sample sintered at 4 GPa, 1673 K is too large for the straight-line approximation in the Williamson–Hall analysis. However, the d^*-dependent broadening of first- and second-order reflections corresponding to $<111>_{\beta\text{-SiC}}$ and $<001>_{\beta\text{-SiC}}$ (see Table 1) points to the presence of both strains and significant strain anisotropy along $<111>_{\beta\text{-SiC}}$ and

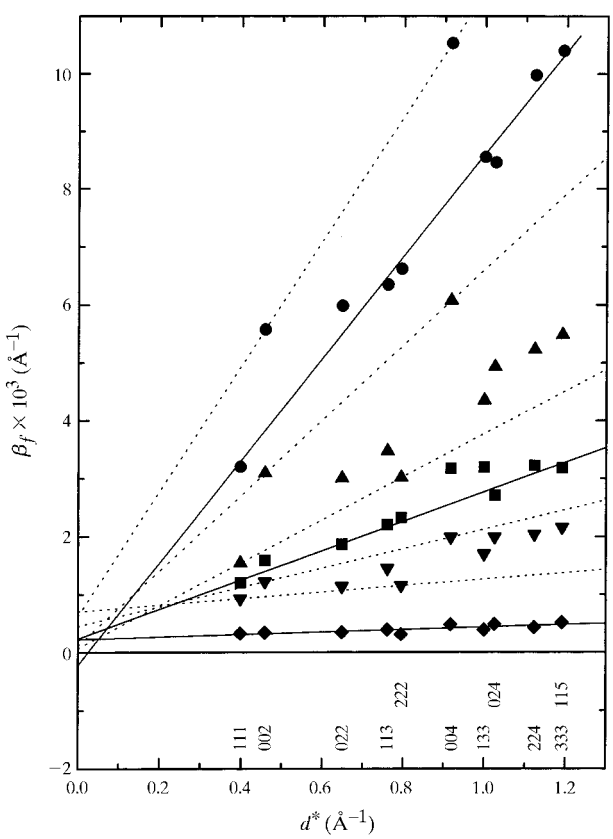

Fig. 6. The integral breadth β_f *versus* d^* plot for line profiles (*hkl* given below) of the as-synthesized SiC–C solid-solution powder (■) and the SiC–C samples sintered at 1673 K [4 GPa (▲) and 8 GPa (●)] and at 2073 K [4 GPa (◆) and 8 GPa (▼)]. Straight-line fits have been used in the Williamson–Hall analysis. Dotted lines correspond to a single cubic structure direction (<111> or <001>).

$<001>_{\beta\text{-SiC}}$ ($e_{WH}<111>/e_{WH}<001>$ = 0.57), which have the largest angle between one another (54.7°) among non-equivalent directions of the cubic structure. The contribution of crystallite size to the reflection broadening is small, as in the as-synthesized powder.

The reasons for such anisotropy after high-pressure sintering are understood. According to Alexander (1986) the anisotropy results from minima of the strong Peierls potential of the covalent crystals, which run parallel to the <011> directions of a cube, as well as the formation and motion of the dislocations in the diamond structure which run parallel to {111} (along <011>), creating the corresponding strain fields. Moreover, the probability of their appearance in this situation is increased by the carbon interlayers located in the cubic SiC structure parallel to {111}. The superposition of the strain fields created within each of the four planes of {111} apparently leads to the largest displacement ($\Delta d/d$) along fourfold symmetry axes ($<001>_{\beta\text{-SiC}}$). Thus, along $<001>_{\beta\text{-SiC}}$ the highest e_{WH} will be fixed. Similar behaviour of the strain parameters is observed in our experimental data (see Table 1 and Fig. 6). The conformation of such strain anisotropy is given by the β_f values for other diffraction peaks. For instance, β_f of the 133 profile corresponding to <133> [forms among non-equivalent directions, one of the lowest angles with <111> (22.0°) and the highest angle with <001> (46.4°)] should be located closer to the straight line plotted through β_f corresponding to <111> (Fig. 6).

It should be noted that the sintering of the normal β-SiC powder [a = 4.359 (1) Å, grain size < 5000 Å and stacking faults present] in the same region creates a strain anisotropy like that mentioned above, but the ratio $e_{WH}<111>/e_{WH}<001>$ is not less than 0.66. Thus, the lower ratio (0.57) for the SiC–C solid solution points to a higher degree of strain anisotropy. The carbon interlayers in the SiC–C solid solution apparently cause an additional strain anisotropy in the process of sintering.

At higher sintering pressure (8 GPa, 1673 K) the strain anisotropy decreases ($e_{WH}<111>/e_{WH}<001>$ = 0.81, closer to 1 than for samples sintered at 4 GPa). An additional mechanism of the dislocation formation which blurs out the anisotropy is probably included in the heavily deformed crystals.

Sintering at the same pressure but at higher temperature (2073 K) leads to some different results, although the strain anisotropy is also observed, especially for the sample sintered at 8 GPa ($e_{WH}<111>/e_{WH}<001>$ = 0.33, see Table 1). The strain parameter of these sintered samples decreases compared with that for the as-synthesized powder, while the strains are not observed in the sample sintered at lower pressure. However, unlike the annealed samples (see §3.2), the decrease of the strains is not accompanied by an increase of the lattice parameter. Thus, sintering at 2073 K reduces the concentration of the second-class (infinite) defects and maintains the first-class (point) defects, while the second-class defects are not present in the sample sintered at 4 GPa, 2073 K. The most likely process leading to such microstructural changes is thermal diffusion. The diffusion coefficient of the superstoichiometric C atoms increases with temperature leading to the destruction of the carbon interlayers (see the structural model suggested in §3.1) and thereby to the disordering of the point defects originally located in the planes (Fig. 5*b*). Different local environments of the superstoichiometric C atoms can be realized in this process [see Fig. 5*c*, (i)–(iii)] and only the first, (i), corresponds exactly to C_{Si}.

An additional weak effect should be noted here: the reduction of the second-class defect concentration is followed by a decrease of the lattice parameter (see Table 1). This effect is apparently connected with the changes in the local environment of the superstoichiometric C atoms in the second coordination sphere induced by the destruction of the carbon interlayers (compare Fig. 5*a* and Fig. 5*b*). Thus, the persistence of the carbon interlayers in the SiC–C structure after high-pressure sintering at the lower temperature (1673 K) promotes the formation of the additional second-class defects. At the same time, the intensified diffusion processes at the higher sintering temperature (2073 K) break down the carbon interlayers and, consequently, reduce the probability of the dislocation formation along the interfaces between the carbon interlayers (C—C) and the silicon carbide layers (Si—C).

4. Concluding remarks

The results obtained allow us to estimate the amount of superstoichiometric C atoms in the SiC structure. Wang *et al.* (1988) pointed out that the relaxation of the atoms around the C_{Si} anti-site defect is 8%; that is, the interatomic distance decreases from 1.88750 (3) Å (for Si—C) to 1.73650 (3) Å (for C—C). Apparently, any grouping of the C_{Si} (carbon interlayers or clusters) changes this value. Therefore, in our case these data could be used correctly only for the sample sintered at 4 GPa, 2073 K, where superstoichiometric C atoms are distributed randomly and do not group into planar defects creating strains.

It is assumed that the C—C bond formation changes only the distances between atoms located in the first coordination sphere. Thus, in order to decrease the lattice parameter from 4.35899 (8) to 4.35234 (5) Å the ratio of the number of Si—C bonds directed along <111> to the number of C—C bonds must be near 98:2. Because one C_{Si} forms four C—C bonds directed along <111> [Fig. 5*c*, (i)], the dissolution of C atoms in the silicon sublattice of SiC is near 0.5 at.%. However, in the real structure, besides an environment of four carbons (C_{Si}) other types of local environment can be found [see Fig. 5*c*, (ii) and (iii)], where only two or three C—C

bonds are present. Therefore, the average number of C—C bonds corresponding to one point defect is three and the dissolution of the superstoichiometric C atoms should be higher: 0.7 at.%. Thus, the composition of the solid solution in the sample sintered at 4 GPa, 2073 K is $Si_{1-x}C_{1+x}$, where $x = 0.007$. Since the lattice parameter does not increase on high-pressure sintering, the dissolved carbon does not leave the structure in the process of sintering and, apparently, this composition also characterizes the as-synthesized solid solution.

According to the suggested structural model (Fig. 5*a*) the superstoichiometric C atoms in the as-synthesized powder are arranged as interlayers along {111}. Thus, the ratio of the C—C layers to the Si—C layers in the SiC–C structure is 7:993. If all C—C defect layers have only one orientation (perpendicular to one of <111>) then the average distance between them is 1000 × 2.514 Å/7 = 360 Å, where 2.514 Å is the distance between the layers. At such an orientation the cubic structure should become hexagonal. However, this is not observed experimentally. Therefore, the existence of C—C layers along each of the four {111} planes is of equal probability and the average distance between these layers along one of <111> is four times higher: 1440 Å. The value obtained correlates well with the SiC crystallite size in the powder after annealing at 1973 K [1875 (208) Å, see §3.2]. It confirms that the SiC–C particles break down along the C—C defect layers during the vacuum annealing process. The small discrepancy between these values is probably connected with resublimation processes, which are strong in SiC powder at this temperature (1973 K), leading to grain growth (Bootsma *et al.*, 1971).

The suggested structural model of the SiC–C solid solution based on carbon interlayers and average distances between the interlayers as estimated above allows a discussion of the Williamson–Hall strain parameter (e_{WH}) for as-synthesized SiC–C with the strain-field model recently suggested by van Berkum *et al.* (1996). The model allows a straightforward calculation of diffraction-line profiles and their characteristics, in particular, integral breadth. The parameters of the model are the average distance between the defects $\langle D\rangle$ (in the case of planar defects this is the distance between the defects in the diffraction-vector direction), the extent of the distortion field w (half width at half height of the strain-field function of the individual lattice defects) and the mean-squared strain $\langle e^2\rangle^{1/2}$.

It is assumed that in our case $\langle D\rangle$ = 360 Å (for simplicity this value is accepted for all crystallographic directions) and a reasonable value for w is $\langle D\rangle/10$ = 36 Å ($w_r = w/\langle D\rangle = 0.1$). The dependence of $\beta_f\langle D\rangle$ *versus* $d^*\langle D\rangle\langle e^2\rangle^{1/2}$ is shown by the curve in Fig. 7 (the Gaussian probability density of strain amplitudes is considered). There are two intervals where a straight-line approximation could be used. Because the line approximation is suitable for the integral widths of the reflections of the as-synthesized powder (Fig. 3) the experimental points must belong to one of the intervals of the straight line. If they belong to the first area, the Williamson–Hall analysis (see line 1 in Fig. 7) attributes the calculated line broadening partly to strain and partly to size: $D_{WH} \simeq 550$ Å. Our results (Fig. 3) do not give such a small crystallite size for the as-synthesized powder (intercept near zero and $D_{WH} > 2000$ Å). The second area is preferable. In this case the Williamson–Hall plot gives a negative intercept (see line 2 of Fig. 7); however, the crystallite size and stacking-fault broadening observed for as-synthesized SiC–C (see §3.1) is not included here. Their addition to the strain broadening shifts line 2 up and the intercept can become positive, like our result (Fig. 3). Since the experimental widths of the as-synthesized powder fit the calculated curve it is concluded that $\langle e^2\rangle^{1/2} = 0.76 \times 10^{-3}$, and size and stacking-fault broadening ($\beta^S = 0.734 \times 10^{-3}$ Å^{-1}) are excluded (see the squares on Fig. 7).

The calculations presented here show that Williamson–Hall analysis can be used for qualitative

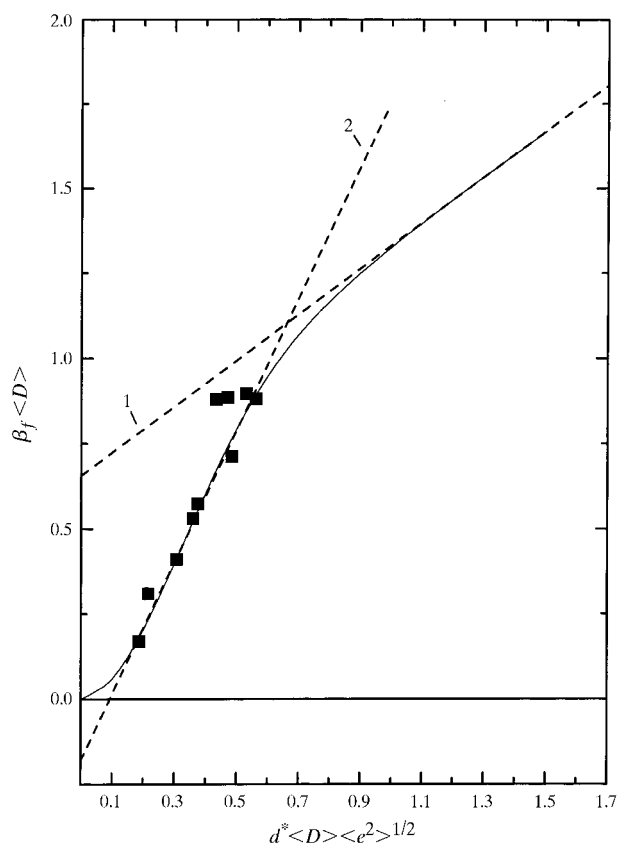

Fig. 7. Calculated relative integral breadth $\beta_f\langle D\rangle$ of line profiles in reciprocal space as a function of $d^*\langle D\rangle\langle e^2\rangle^{1/2}$ for width $w_r = 0.1$ of the component strain fields (solid curve) and integral breadth of the as-synthesized SiC–C diffraction peaks reduced to the strain-field model parameters $\langle D\rangle$ = 360 Å, $\langle e^2\rangle^{1/2} = 0.76 \times 10^{-3}$ and $w_r = 0.1$ (■). The dashed lines (1 and 2) are discussed in the text.

microstructure investigations of the SiC–C solid solution. The value of the strain parameter e_{WH} is higher than the mean-squared strain $<e^2>^{1/2}$, although as w_r tends to ∞ $<e^2>^{1/2}$ tends to e_{WH}. Additionally, calculations of the integral width based on the strain-field model allow us to remove the contradiction between the rather significant value of D_{WH} (this value includes both size and stacking-fault broadening) and the presence of stacking faults in the structure of as-synthesized SiC–C, since $1/D_{WH}$ should not be counted from zero, as usual in Williamson–Hall analysis, but from the intercept of the strain-broadening line in the negative region (see line 2 of Fig. 7) and, therefore, for the as-synthesized powder D_{WH} = 1360 Å. The contribution of size and stacking-fault broadening could then be significant in profiles in the small-2θ-angle zone; this is confirmed by the size-dependent Lorentzian shape of the peaks seen here (see §3.1).

In general, the following conclusions can be made:

(i) A crystal structure model of SiC with superstoichiometric carbon is proposed. The model is based on the location of carbon along close-packed {111} planes of silicon carbide.

(ii) It is shown that the C atoms in the β-SiC structure are arranged either as infinite defects (diamond-like carbon interlayers) after synthesis or as non-correlated point defects (in particular, C_{Si}) after sintering of the as-synthesized powder at high pressures (4–8 GPa) and temperature (2073 K).

(iii) The SiC–C solid solution disintegrates under vacuum annealing in the temperature range of diamond graphitization; this change is accompanied by a lattice-parameter increase [from 4.3540 (2) to 4.35899 (8) Å], a decrease in microstrains and a decrease of crystallite size; at the same time the superstoichiometric C atoms persist in the SiC structure on sintering at high pressures (4–8 GPa) and temperatures (1673–2073 K).

The authors thank Dr O. O. Bochechka for his help in the preparation of the sintered samples.

References

Akselrud, L. G., Grun, Yu. N., Zavalii, P. Y., Pecharskii, V. K. & Fundamentskii, V. S. (1989). *Twelfth European Crystallographic Meeting Collected Abstracts*, Vol. 3, p. 155. Moscow.

Alexander, H. (1986). *Dislocations in Solids*, Vol. 7, edited by F. R. N. Nabarro, pp. 113–234. Amsterdam: Elsevier.

Berkum, J. G. M. van, Delhez, R., de Keijser, Th. H. & Mittemeijer, E. J. (1996). *Acta Cryst.* A**52**, 730–747.

Bonnke, M. von & Fitzer, E. (1966). *Ber. Dtsch. Keram. Ges.* **43,** 180–187.

Bootsma, G. A., Knippenberg, W. F. & Verspui, G. (1971). *J. Cryst. Growth*, **8**, 341–353.

Evans, T. & James, R. A. (1964). *Proc. R. Soc. London Ser. A*, **277**, 260–269.

Gadzyra, N. F., Gnesin, G. G., Andreyev, A. V., Kravets, V. G. & Kasjanenko, A. A. (1996). *Inorg. Mater.* **32**, 721–725.

Kennedy, C. S. & Kennedy, J. C. (1976). *J. Geophys. Res.* **81**, 2467–2470.

Khaenko, B. V., Prilutskii, E. V., Mikhailik, A. A., Karpets, M. V. & Krainikov, A. V. (1995). *Inorg. Mater.* **31**, 304–309.

Krivoglaz, M. A. (1996). *X-ray and Neutron Diffraction in Nonideal Crystals*, pp. 33–56. Berlin: Springer.

Lely, J. A. (1955). *Ber. Dtsch. Keram. Ges.* **32**, 229–331.

Olesinski, R. W. & Abbaschian, G. J. (1984). *Bull. Alloy Phase Diag.* **5**, 486–489.

Pujar, V. V. & Cawley, J. D. (1995). *J. Am. Ceram. Soc.* **78**, 774–782.

Rafaniello, W., Cho, K. & Virkar, A. V. (1981). *J. Mater. Sci.* **16**, 3479–3488.

Shaffer, P. T. B. (1969). *Mater. Res. Bull.* **4**, 97–106.

Sorokin, N. D., Tairov, Y. M., Tsvetkov, V. F. & Chernov, M. A. (1983). *Kristallografiya*, **28**, 910–914.

Tateyama, H., Sutoh, N. & Murakawa, N. (1988). *J. Ceram. Soc. Jpn Int. Ed.* **96**, 985–994.

Wang, C., Bernholc, J. & Davis, R. F. (1988). *Phys. Rev. B*, **38**, 12752–12755.

Warren, B. E. (1969). *X-ray Diffraction.* Reading, MA: Addison–Wesley.

Wei, G. C., Kennedy, C. R. & Harris, L. A. (1984). *Am. Ceram. Soc. Bull.* **63**, 1054–1061.

Williamson, G. K. & Hall, W. H. (1953). *Acta Metall.* **1**, 22–31.

Wilson, A. J. C. (1962). *X-ray Optics.* London: Methuen.

Yurkovskii, I. M., Smirnova, T. Y. & Malei, A. S. (1986). *Khim. Tverd. Topl.* **1**, 127–131.